Co-funded by the European Union

TE@CH

additive manufacturing academy
TO BOOST trainers' competences in industry

Summary

Design for Additive Manufacturing (DfAM)

Project Number: 2021-1-IT01-KA220-VET-000033365

TE@CH

UNIT 4 – MECHANICAL BEHAVIOR

Course Content

The fourth unit of module two is about the mechanical behaviour; in particular the mechanical behaviour of AlSi10Mg lattice structures manufactured by the Selective Laser Melting (SLM)

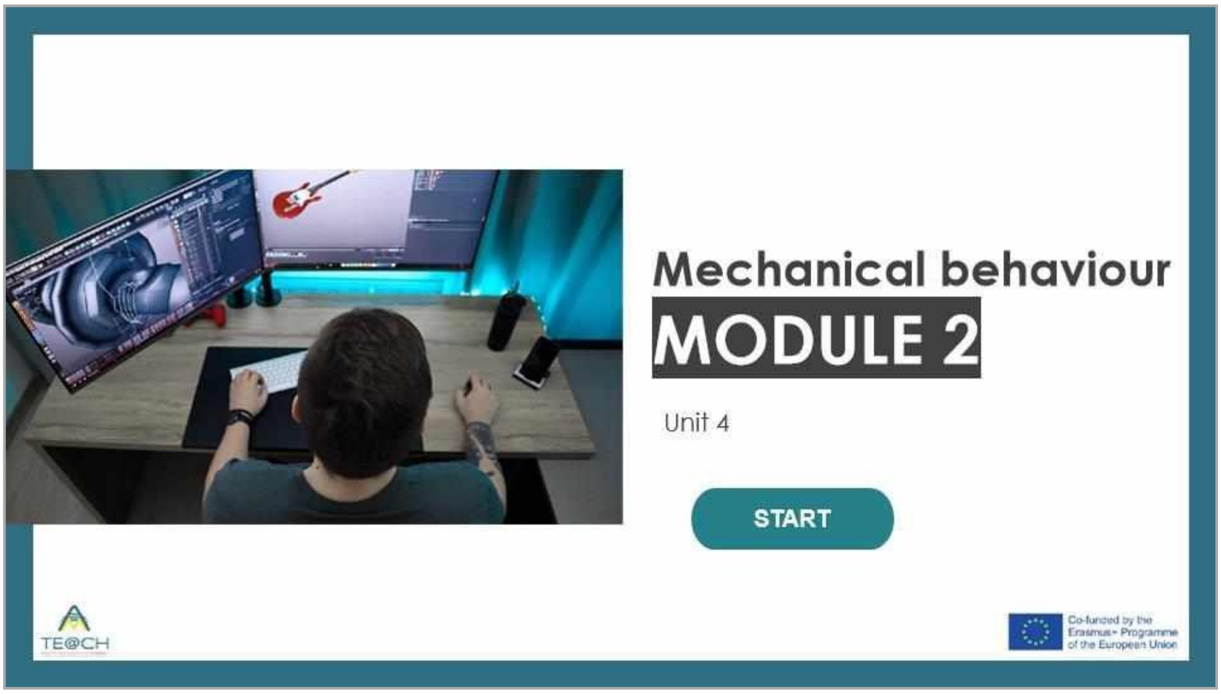

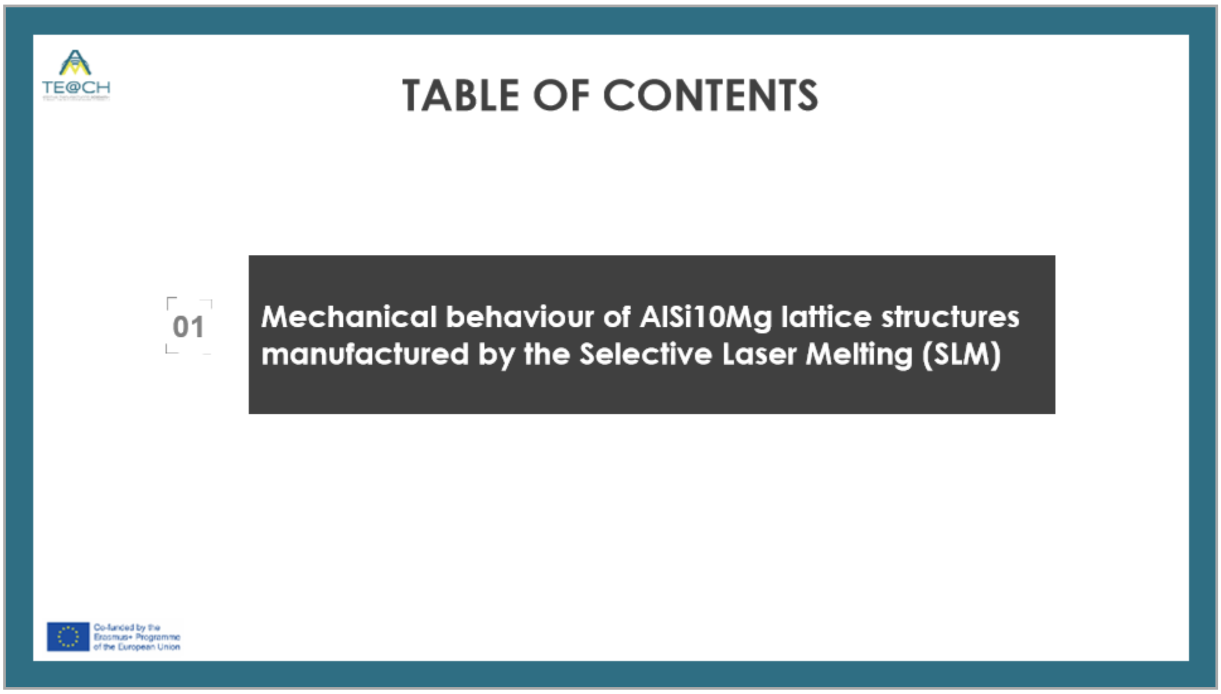

INTRODUCTION

Selective laser melting (SLM) is an additive manufacturing process in which part geometry is progressively built up by selectively melting layers of metal powder, using a scanning laser beam under inert gas atmosphere, with elevated precision and freedom of design, particularly for the internal details.

TE@CH

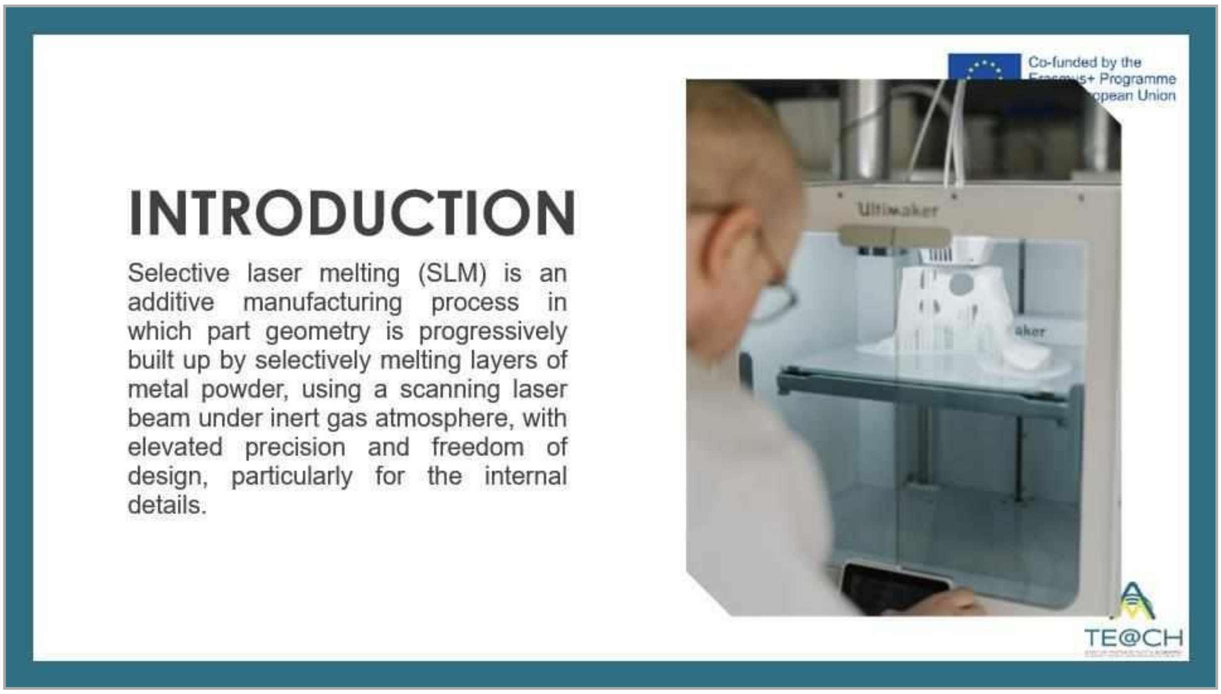

In this unit we can learn to know the characteristics of technologies using powders, e.g. selective laser sintering (SLS), consolidation of powders with a binder (3D-Printing), selective laser melting (SLM).

LATTICE SAMPLES

Additive manufacturing (AM), particularly Selective Laser Melting (SLM) has enabled design and production of complex metal lattice structures with specifically required properties, minimizing weight. The aim of this work is to provide insight into the influence of cell topology, cell size and beam diameter on deformation and failure behaviour of different SLM-manufactured AlSi10Mg alloy structures under static compressive loading. Design of Experiment (DOE) analysis is performed to define geometrical features and dimensional characteristics of cell unit for specimen final configuration. A total of sixteen topological combinations was obtained and forty-eight lattice specimens with three replicas for each cell type were manufactured with random order process to minimize manufacturing time variation and dependence. The full experimental testing results were analysed and compared in absolute terms and related to lattice density. Furthermore, a deep experimental microscopic analysis was conducted for a statistical analysis of representative beam diameters and real cell sizes for lattice samples. Additionally, micro-computed tomography (micro-CT) inspection was employed to analyse the local morphology and to characterize material distribution and in particular to verify defect presence (such as porosity and superficial anomalies) that may affect the mechanical behaviour. As for the orientation of the pieces of the present work, the pre-processor of the 3D printing machine (Renishaw AM400) was used. Of all the lattice structures, the only one that required a major study was SC_8_1, characterized by maximum cell size (8mm) and minimum beam diameter (1mm). In this case, the Figure 4 (c) represents the optimal build orientation of SC_8_1 lattice structures, placing it in one point and inclined at about 45 °.

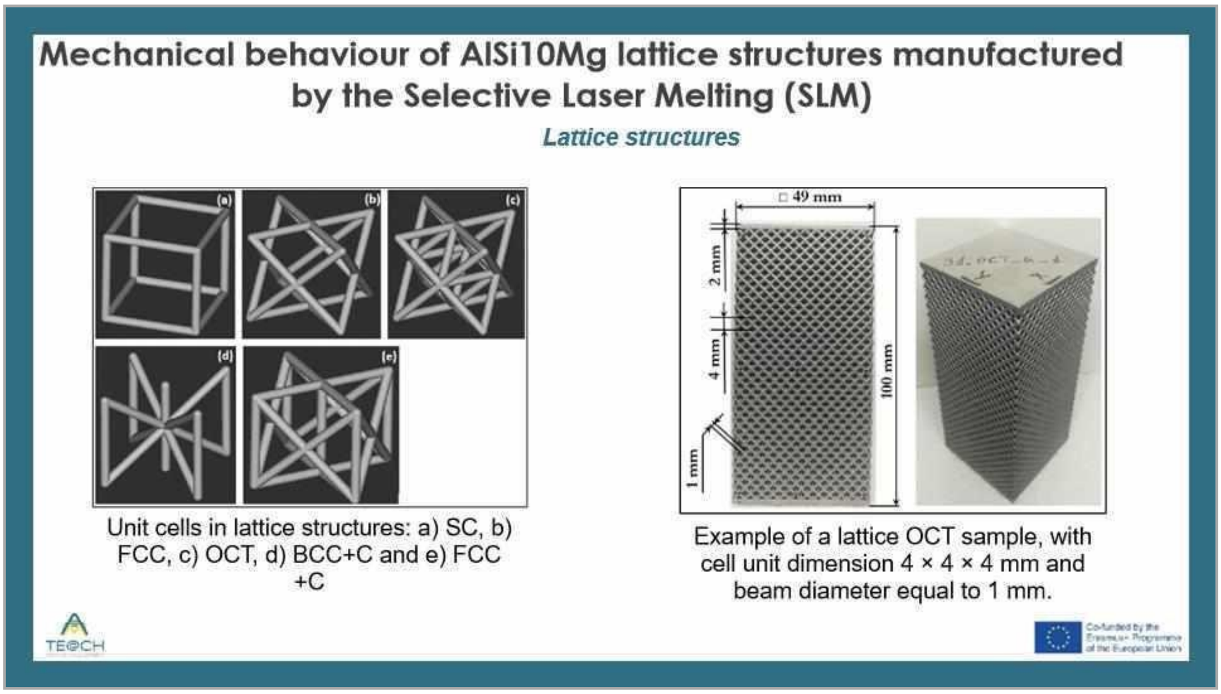

LATTICE STRUCTURES

Unit cells in lattice structures: a) SC, b) FCC, c) OCT, d) BCC+C and e) FCC+C. Example of a lattice OCT sample, with cell unit dimension 4 × 4 × 4 mm and beam diameter equal to 1 mm.

The 'strut-based' geometries seem to represent the most promising lattice configurations for simpler additive process and lower cost, with respect to Shell or TPMS lattice configurations.

Different 'strut-based' lattice structures are selected afternumerical simulation for proper structural behaviour under compressive loads. The designed lattice structures consist of Simple Cubic (SC), Body Centred Cubic + Columns (BCC+C), Face Centred Cubic (FCC), Octet (OCT) and Face Centred Cubic + Columns (FCC+C), as illustrated in Figure.

Different simulations have been performed on lattice specimens with a theoretical global dimension of 48 × 48 × 96 mm.

Two continuous flat bases of thickness equal to 2 mm are added at extremities of these samples and manufactured with the same material. The section of samples is selected based on the overall dimensions of structure. Therefore, the final dimensions are selected after initial definition of three configurations for beam thicknesses and cell dimensions, considering also the five lattice topologies, as shown in Figure, where stiffness/mass ratios are considered.

The total volumes are equal to 49 × 49 × 100 mm3, 49.5 × 49.5 × 100 mm3 or 50 × 50 × 100 mm3 for lattice samples with beam diameter equal to 1 mm, 1.5 mm, or 2 mm, respectively; a representative example of lattice configuration is reported in Figure with relevant dimensions.

In addition, a statistical technique denotated as Design of Experiment (DoE) is conducted aided by the Analysis of Variance (ANOVA) after the numerical procedures to investigate the suitable configuration of specimens for compressive characterization along the two main directions (X and Z axes). Specifically, the DoE method includes different statistical methodologies employed to evaluate parameters combinations and main factors influence for the optimization and improvement of a specific process. In the present work, the DOE was implemented to select proper features of lattice specimens for compressive testing.

The most influential input factors for the stiffness along X / sample mass response are:

- Cell topology: BCC+C and OCT
- Cell size: 4 and 8 mm
- Beam diameter: 1 and 2 mm.
- Instead, the input factors that most influence the stiffness long Z / sample mass response are:
- Cell topology: FCC+C and SC
- Cell size: 4 and 8 mm
- Beam diameter: 1 and 2 mm.

Therefore, a total of 16 topological combinations is obtained by the DoE results and 48 lattice specimens with three replicas for cell type are manufactured through a randomization process in order to minimize noise and process dependence.

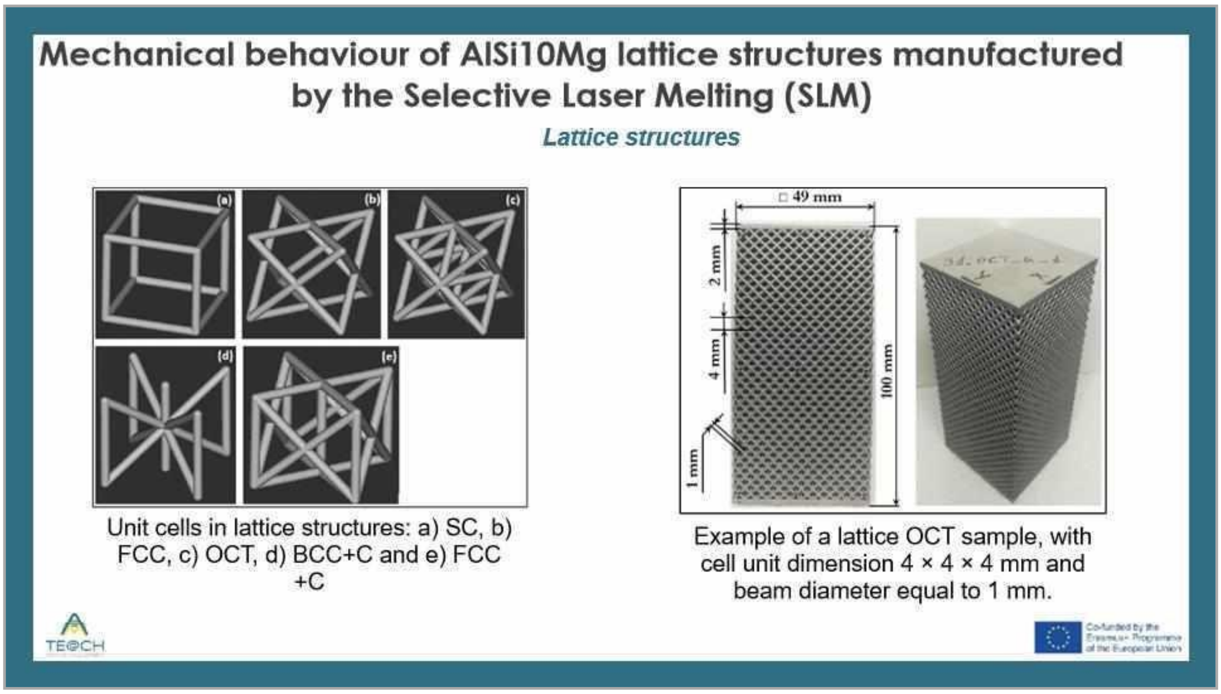

CELLULAR PROPERTIES OF LATTICE SAMPLES

The Table reports the lattice features in terms of cell type, cell dimensions and beam diameter of different sample batches employed for compressive tests, showing the front views of the specimen type. The four cellular topologies employed for the tested samples include the BCC + C, the FCC + C, the OCT and the SC elements

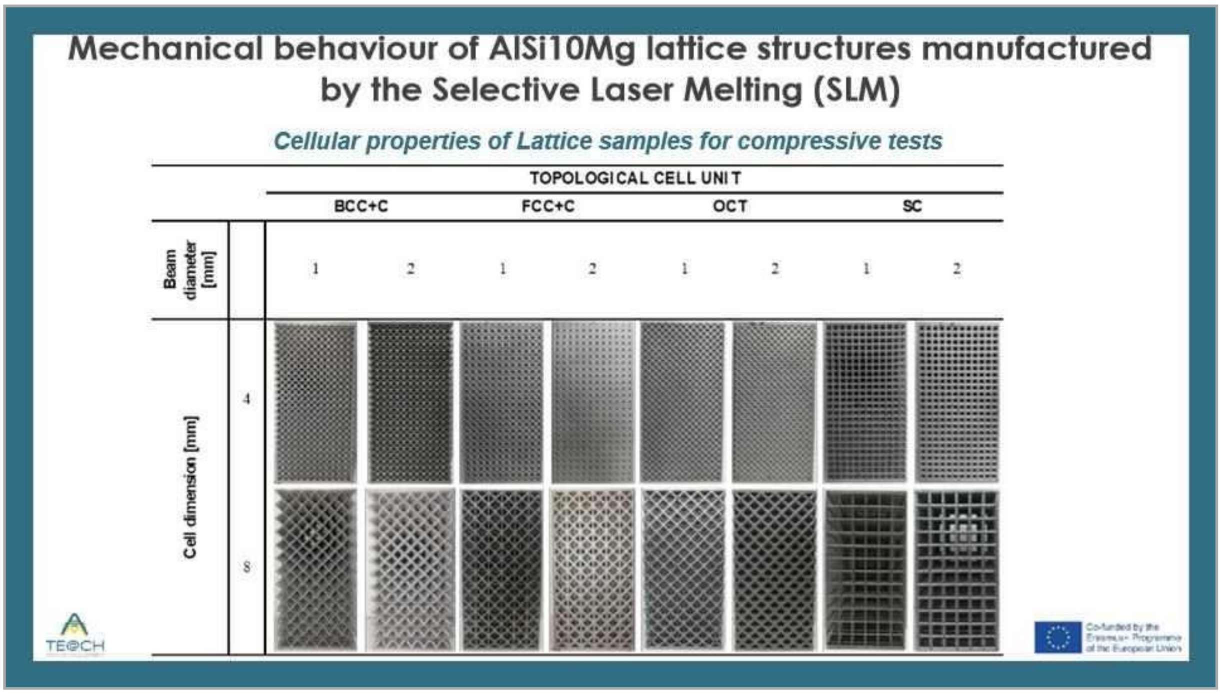

MICROSCOPIC ANALYSIS

In addition, an experimental microscopic analysis was performed to evaluate the mean value and relative percentage deviation of beam diameter and cell size measurements for selected lattice samples. Figure shows the experimental microscopic setup where the lattice sample is positioned under the plain base after remoting the circular slim base to optimize optical objective – sample distance. The Stereo-microscope Nikon SMZ 1000 was employed for the high-resolution detection and zoom magnification of selected cell units in combination with imaging software NIS Elements to calibrate and to acquire image data.

Figure shows a representative example of reference system selected for a FCC + C cell topology where beams diameters and cell dimension could be assessed in the YZ plane.

The zoom magnifications highlight the horizontal arrangement of sample during the dimensioning phase. An evident widespread roughness is observed on the surface of oblique beams due to the powder's adhesion during manufacturing process. Obviously, this phenomenon affects remarkably on beams and cell sizing. However, if the beam diameter increases, it is observed that this adhesion effect of metallic powder could provide a very dense cells that also the microscopic measurement result so difficult due to indistinguishable surfaces of beams.

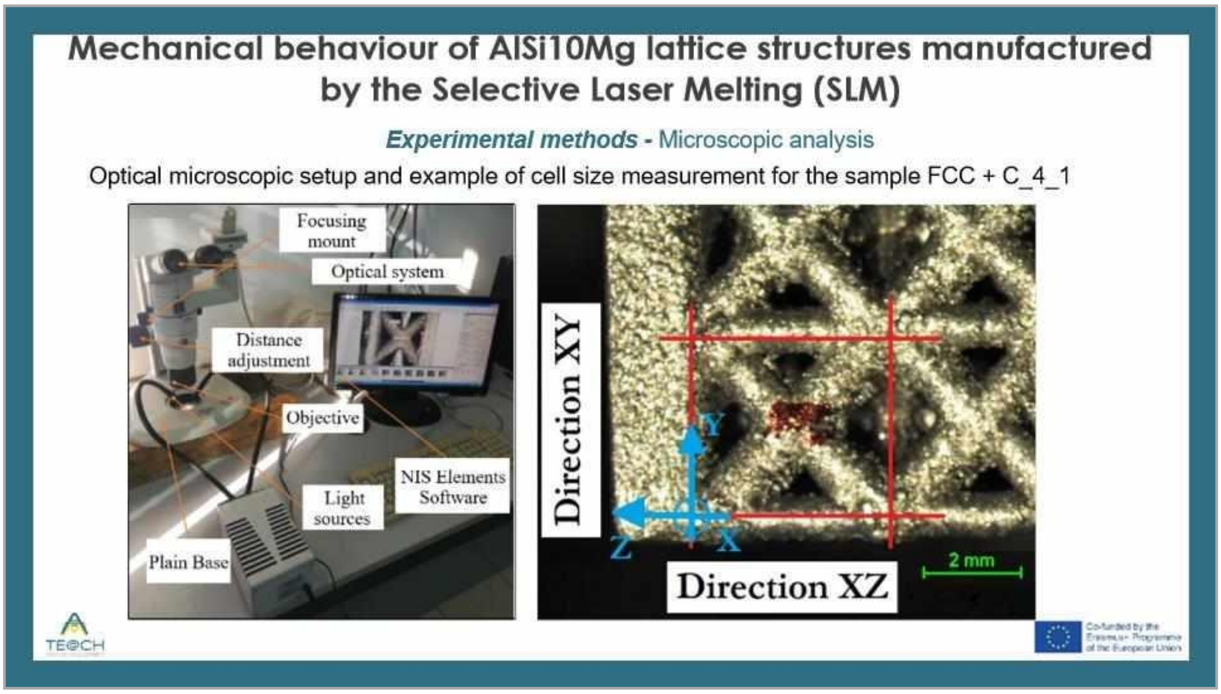

Example of microscopic analysis.

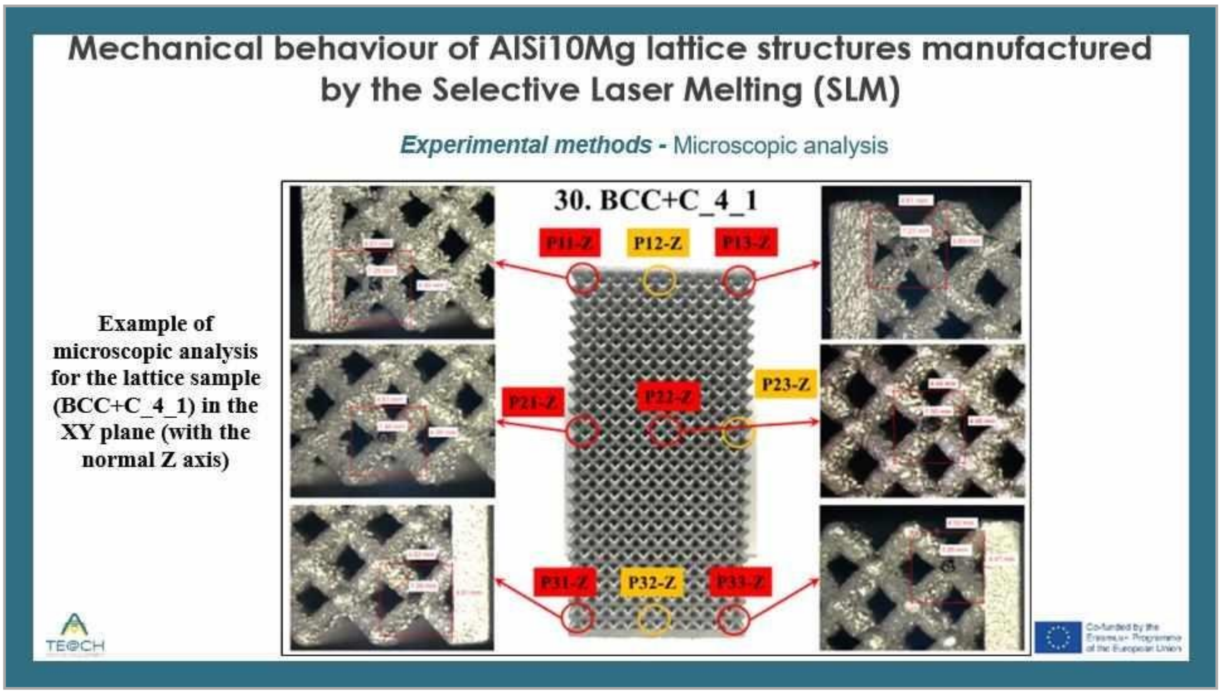

Specifically, the microscopic measurements were assessed on 9 points were different cells are located on two adjacent lateral surfaces of each lattice specimen, arranged and indicated as shown in Figure. Therefore, the measured cell units are positioned only on the external surface of samples and aligned on the extremities and in central zone close to the upper aluminium plate, the central section and lower plate for a proper and discrete dimensional characterization.

X-RAY MICRO-TOMOGRAPHY EVALUATION

The micro-CT analyses were performed in the laboratory of the ENEA® - National Agency for New Technologies, Energy and Sustainable Economic Development at Brindisi (Italy). A GE Phoenix Nano-tom CT system equipped with a 180 kV/15 W nano-focus X-ray tube, a precision rotary table on air bearings, and a 2300 × 2300 pixels Hamamatsu flat panel detector was used.

Specifically, the number of pores in the BCC_C samples is approximately an order of magnitude greater than that observed in the SC samples.

However, an interesting uniform distribution of porosity is noted inside both types of lattice structures for the representative BCC+C and SC elements, respectively. Furthermore, in all the observed samples, the voids seem to be characterized by a spherical shape (sphericity greater than 0.918) and by an equivalent mean diameter of about 60 µm.

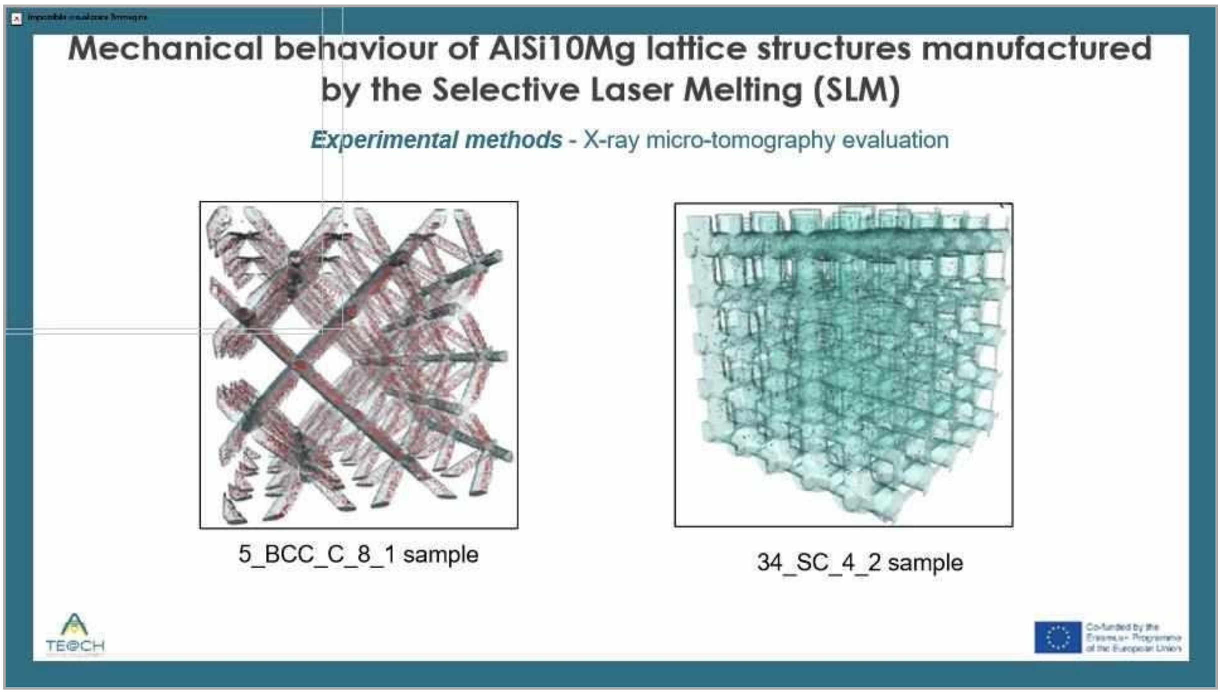

EXPERIMENTAL AND MONITORING PROCEDURES

The compressive and tensile static tests are performed on a servo-hydraulic testing machine - INSTRON Model 8850 with a load cell of ± 250 kN, as shown in Figure. Specifically, compressive experimental tests are performed according to the ASTM E9 – 09 (Standard Test Methods of Compression Testing of Metallic Materials at Room Temperature) by placing the specimen between two steel compression platens, as reported in Figure.

The goal of this methodology is to obtain an innovative concept that guarantees the same or better stiffness but allows to obtain a weight reduction.

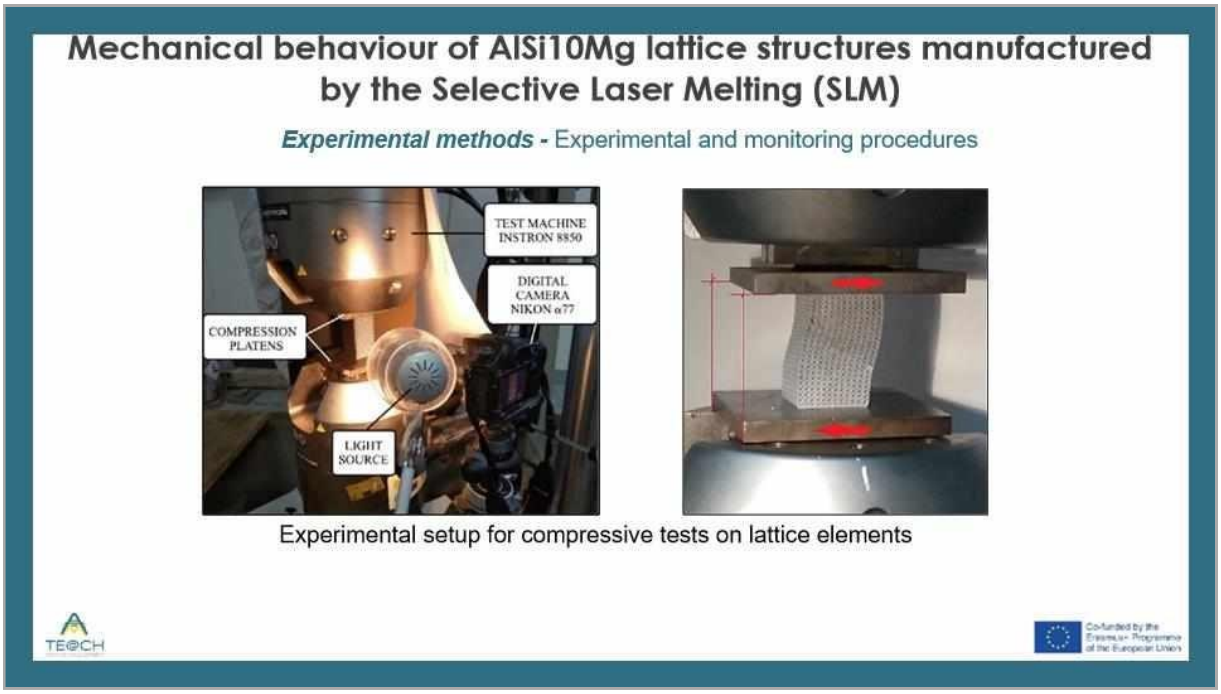

RESULTS AND DISCUSSION

In Figure the Stress-strain curves are reported for different lattice elements with the topological BCC+C cell unit, where a similar mechanical behaviour both in the elastic and plastic region is observed in both BCC + C_8_2 and BCC + C_4_1 samples, except for the specimen ID 30.BCC + C_4_1. The σ - ε curves present a linear elastic region followed by a wide plastic zone with a slight reduced slope, before the sudden stiffness reduction due to the failure of slicing plane [45 °]. During the initial loading phase, a greater linear elastic section followed by a subsequent very reduced plastic area and then sudden yield is observed.

The same deformation phenomenon occurs in each cell under compressive loading and a greater strain range is observed. In the first phase before the first collapse of lattice cell level, while a strain reduction is noted in the subsequent plastic section after the failure of the first unit level, due to the previous permanent damages.

The trend of the curves is typical of a bending - dominated behaviour showing a plateau phase in the plastic field, but the irregular absence of the densification zone is noted in the trend behaviour. However, the trend of plastic regions and relative strain data results variable, especially for the specimen ID 30.BCC + C_4_1 that highlights stress values and a mechanical behaviour different from the other two BCC+C_4_1 elements. In fact, the ultimate stress of sample ID 30.BCC + C_4_1 is higher roughly 1.5 times than the other tested specimens.

Moreover, higher data results are observed for the sample ID 30.BCC + C_4_1, whilst an almost uniform waveform whilst the σ-ε curve of sample ID 1.BCC+C_8_2 highlights different plastic regions after the first elasto-plastic phase with almost uniform waveforms that reaches a final maximum strain equal to 0.286 [mm/mm].

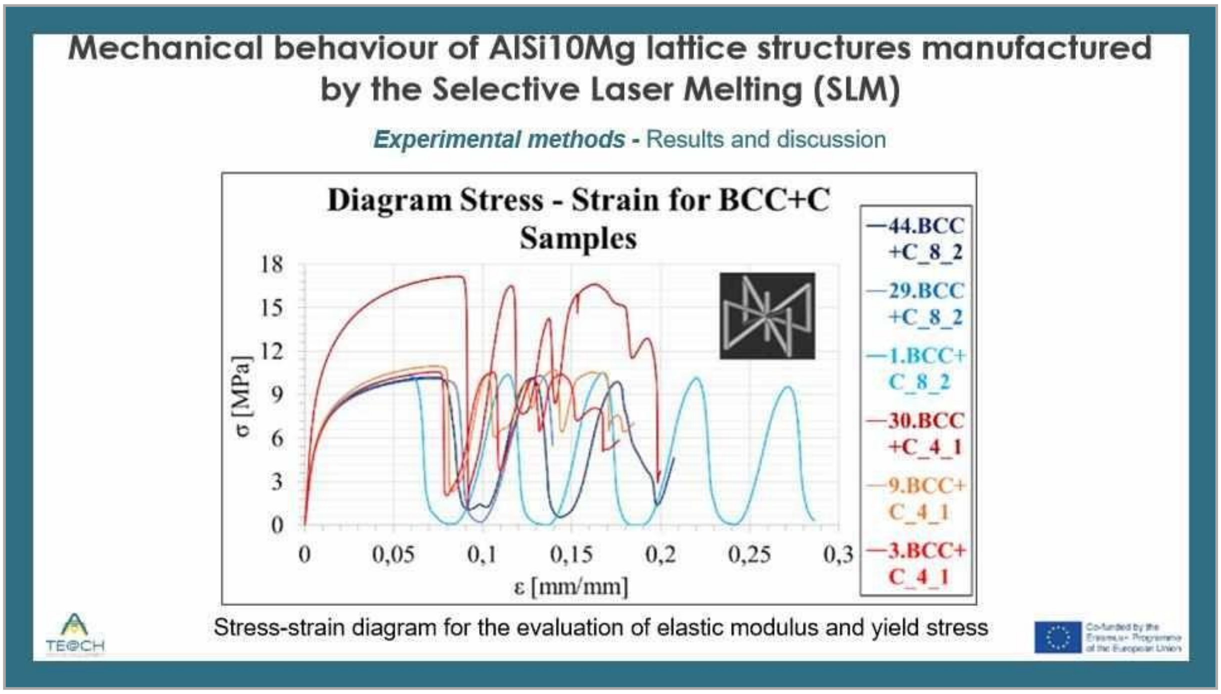

Thus, for a proper comparative analysis, the mechanical properties are evaluated from the specific stress-strain curves of BCC+C elements highlighting the comparable results of cell topology, except for the specimen ID 30.BCC + C_4_1, as shown in the histograms of Figures (a), (b) and (c).

However, in the histogram of Figure (c), the compressive strength related to the first peak of σ-ε curve and the maximum stress values are compared showing that only two of three samples with BCC+C_8_2 cell unit exhibits the maximum stresses after the first peak due to the densification phenomenon during the compression loading.

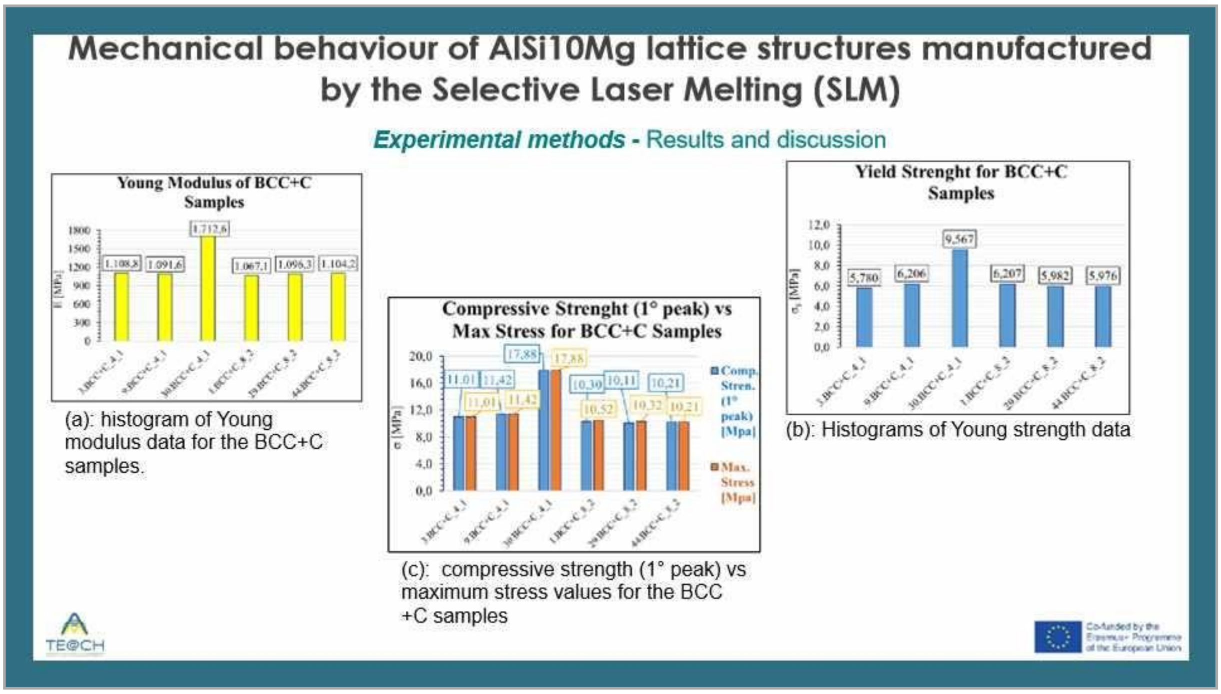

The damage initiations and progressive propagations are monitored during the compressive tests of each BCC+C samples and correlated to the specific stress-strain diagrams, as shown in example Figures (a) and (b) for ID 44.BCC+C_8_2 and ID 3.BCC+C_4_1 elements.

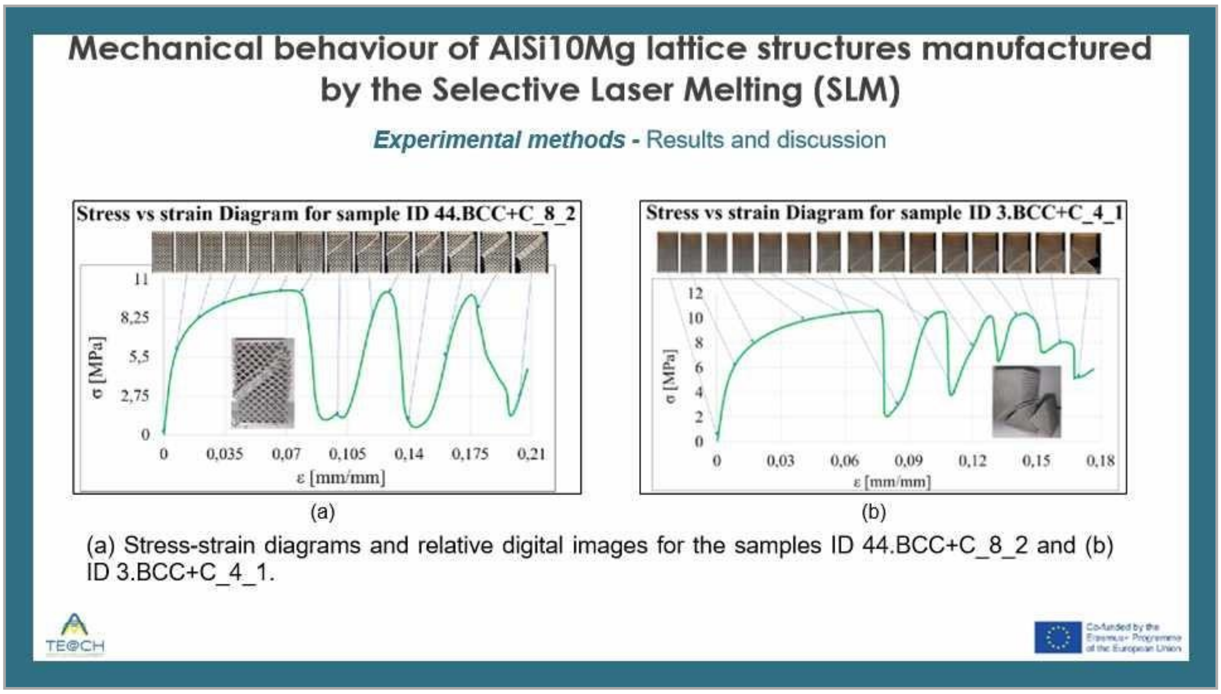

Also in Table, the damage initiation and progression are reported fir these representative BCC+C samples. Similar damage modes until the final failure are observed for the other BCC+C elements. During the compression tests, a continuous deformation of tested lattice element is observed until the first deformation in a barrel-like manner of lattice structure. The lattice cells result deformed in a barrel-like manner owing to the constraints in the X and Y directions on the top and bottom surfaces. A consequent deflection mechanism seems to occur in the unit cells up to the first failure of the lattice plane at 45 ° respect to the loading direction in the plane normal of Z-Axis direction. The cell columns are employed such as an interlock constraint condition of the beams connected up to the central node, avoiding the sliding phenomenon in the plane normal to the Y-Axis direction. Moreover, consequent and progressive damages arise on lattice planes at 45 ° parallel to the first damage direction in the BCC+C_8_2 specimens, as reported in Table.

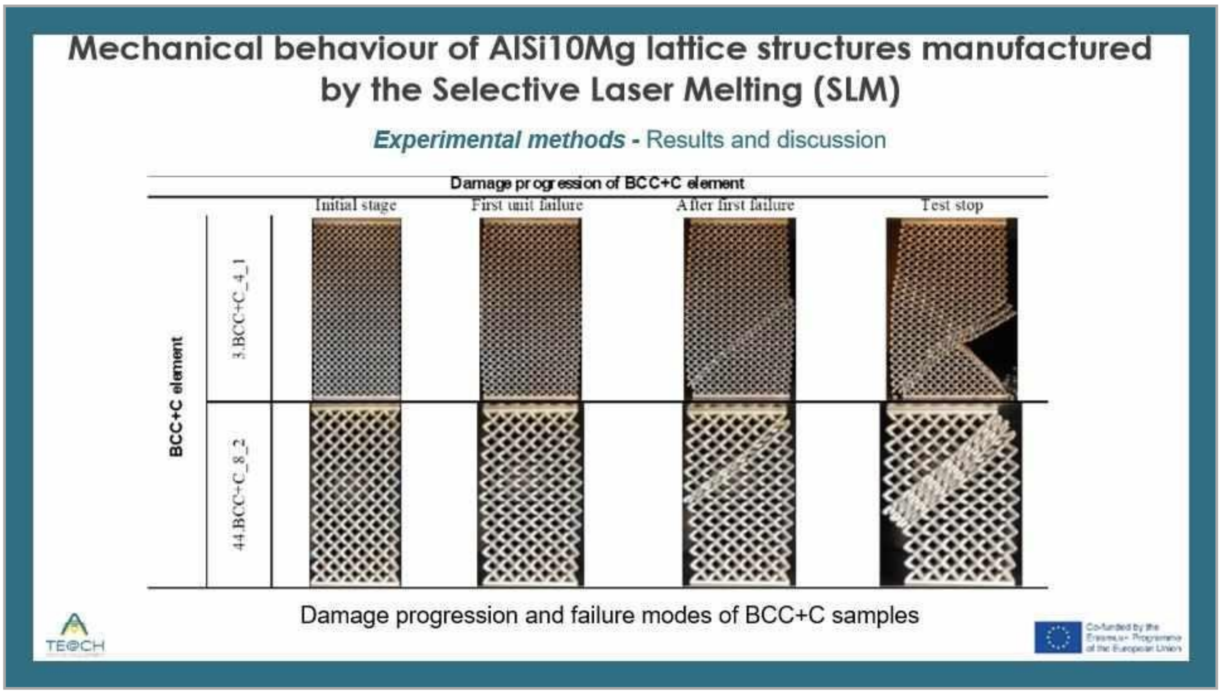

For further information and contact details, have a look here:

ITS Aerospazio Puglia
https://www.itsaerospaziopuglia.it/
Cittadella della Ricerca S.S.7 km 7,300
72100 Brindisi (BR)
Puglia, Italy

University of Salento
Department of Engineering for Innovation
https://www.dii.unisalento.it/
Complesso Ecotekne - Edificio "Corpo O"
Via per Monteroni
73100 LECCE (LE)
Puglia, Italy

Funded by the European Union. Views and opinions expressed are however those of the author(s) only and do not necessarily reflect those of the European Union or the European Education and Culture Executive Agency (EACEA). Neither the European Union nor EACEA can be held responsible for them.